Received: 10 November 2019 | Revised: 1 April 2020 | Accepted: 2 April 2020

DOI: 10.1111/jace.17156

SPECIAL ISSUE ARTICLE

Journal of the American Ceramic Society

Evaluation of isotopic boron (^{11}B) for the fabrication of low activation $Mg^{11}B_2$ superconductor for next generation fusion magnets

Hyunseock Jie PhD[1,2] | **Vladimir Luzin**[2] | **Mukter Zaman**[3] | **Anvar Valiyaparambil Abdulsalam**[1,4] | **Keun Hwa Chae PhD**[5] | **Hyung-il Choi**[6] | **Vladimir Levchenko**[2] | **Arend Nijhuis**[4] | **Jung H. Kim**[1] | **Mislav Mustapić**[7] | **Shi Xue Dou**[1] | **Yusuke Yamauchi**[8] | **Aslam Khan**[9] | **Md. Shahriar A. Hossain**[1,10]

[1]Institute for Superconducting and Electronic Materials, Australian Institute for Innovative Materials (AIIM), University of Wollongong, Wollongong, NSW, Australia

[2]Australian Nuclear Science & Technology Organisation (ANSTO), Lucas Heights, NSW, Australia

[3]Faculty of Engineering, Multimedia University, Cyberjaya, Malaysia

[4]Faculty of Science & Technology, University of Twente, Enschede, The Netherlands

[5]Advanced Analysis Center, Korea Institute of Science and Technology (KIST), Seoul, Republic of Korea

[6]MOP (Mother of Pearl) Co., Ltd, Suwon-si, Republic of Korea

[7]Department of Physics, University of Osijek, Osijek, Croatia

[8]School of Chemical Engineering and Australian Institute for Bioengineering and Nanotechnology (AIBN), The University of Queensland, Brisbane, Qld., Australia

[9]King Abdullah Institute for Nanotechnology, King Saud University, Riyadh, Saudi Arabia

[10]School of Mechanical and Mining Engineering and Australian Institute for Bioengineering and Nanotechnology (AIBN), The University of Queensland, Brisbane, Qld., Australia

Correspondence
Vladimir Luzin, Australian Nuclear Science & Technology Organisation (ANSTO), Lucas Heights, NSW 2232, Australia.
Email: vll@ansto.gov.au

Md. Shahriar Al Hossain, School of Mechanical and Mining Engineering and Australian Institute for Bioengineering and Nanotechnology (AIBN), The University of Queensland, Brisbane, Qld. 4072, Australia.
Email: md.hossain@uq.edu.au

Funding information
Australian Research Council (ARC), Grant/Award Number: LP160101784; Australian Centre for Neutron Scattering (ACNS), Grant/Award Number: ZIAI073441; Australian Nuclear Science and Technology Organization (ANSTO); King Saud University, Grant/Award Number: RSP-2019/127; University of Osijek, Grant/Award Number: ZUP-2018

Abstract

In this study, we analyze the properties of boron isotope (^{11}B)-rich powders from three different sources, that is, American, Cambridge, and Pavezyum, to fabricate the bulk $Mg^{11}B_2$ superconductors and evaluate their superconducting properties. While ^{11}B-rich powder is an essential precursor to fabricate $Mg^{11}B_2$ superconductors for fusion magnet applications, the properties of the ^{11}B powder turned out to be critical to determine the quality of the final superconducting product. Therefore, appropriate control of processing conditions is needed to comply with the requirements of the nuclear fusion application. Analysis of the B isotope ratio by accelerator mass spectroscopy and neutron transmission revealed that all three types of powder are enriched with ^{11}B to better than 99 at % quality. In addition, Pavezyum's ^{11}B shows the lowest crystallinity and smallest crystalline domain size as evidenced by the high-resolution X-ray diffractometer and scanning electron microscopy. The chemical states of the boron isotope investigated with near edge X-ray absorption fine structure spectroscopy and X-ray photoemission spectroscopy also reveals that Pavezyum boron has amorphous structure. $Mg^{11}B_2$ bulks and multi-filamentary (12-filament) wires have

been manufactured, sintered at different temperatures and characterized via the transport critical current density. The wire with Pavezyum ^{11}B shows three times higher current carrying capacity at a particular magnetic field compared to the wire using Cambridge ^{11}B and hence, Pavezyum ^{11}B boron has the potential for manufacturing fusion grade $Mg^{11}B_2$ based magnets. The results of this study demonstrated that Boron powders with higher purity, smaller grain size and lower crystallinity are critical for improving the superconducting and electronic properties of $Mg^{11}B_2$ samples fabricated from the powder. Thus, the low-neutron-activation $Mg^{11}B_2$ is possibly an affordable and technically viable candidate to replace NbTi superconductors in the low field poloidal field and correction coils for the next-generation fusion reactors.

KEYWORDS

boron isotope, critical current density, magnesium diboride, superconductors

1 | INTRODUCTION

Within the scope of the International Thermonuclear Experimental Reactor (ITER) project, Nb_3Sn and NbTi superconducting wires and cables are used as essential constituents of the toroidal field and poloidal field (PF) coils to contain the deuterium-tritium (D-T) fusion plasma.[1-3] Nb-based low temperature superconductors have significant drawbacks. For long-term and steady-state operation of the D-T plasma fusion reactors, it is desirable that the superconducting magnet elements have low neutron activation.[4,5] The Nb-based superconductors, however, require a very long period for the radioactivity to decay and to cool down after neutron irradiation.[6] Thus, this creates an additional problem for the maintenance and treatment of the radioactive wastes.[6] On the other hand, MgB_2-based superconductors have a short decay time and are known as one of the most low activation superconducting materials.[7] Furthermore, MgB_2 superconductors have a higher operating temperature compared to the Nb-based superconductors.[8]

For the purpose of using MgB_2-based superconducting magnets in the fusion reactor, it is necessary to consider the properties of the boron precursor carefully, especially the nuclear properties. Natural boron is a mixture of two isotopes, boron-10 (^{10}B; 20%) and boron-11 (^{11}B; 80%).[9,10] ^{10}B has a very large neutron absorption (capture) cross-section and is usually used as a neutron absorber in nuclear power plants in the radiation shield or control rods.[11,12] In the neutron flux, ^{10}B is transformed to ^{7}Li and He by a neutron reaction ($^{10}B + n, \alpha \rightarrow {}^{7}Li + 4He$).[13-15] In contrast, the ^{11}B isotope is stable with respect to neutron irradiation, lacking the (n, α) reaction, and can reduce nuclear heating.[16-18] Thus, from the practical point of view, the application of ^{11}B based $Mg^{11}B_2$ superconductors is crucial in the neutron irradiation environment, there is a definite requirement of ^{11}B to fully replace ^{10}B.[18] If the problem of ^{11}B enrichment is solved to a practically acceptable degree, we believe that $Mg^{11}B_2$ superconductor is a promising candidate to replace the NbTi superconductors in the low field fusion magnets.

To further improve the superconducting and electronic properties, the quality and requirements of the starting B powders, such as purity, size distribution, and particle size, etc, need to be considered critically as they play an important role[19-25] in determining the fundamental properties of MgB_2. In this paper, we have analyzed the isotopic ^{11}B powder and manufactured the low activation $Mg^{11}B_2$ bulk superconductor and multifilamentary (12-filament) wires using ^{11}B-rich precursors to evaluate the properties which are important for application in superconducting magnets for fusion reactors. Apart from the control of the isotope composition, in the case of the powder precursors, we studied properties that are important for the reaction formation of $Mg^{11}B_2$, such as the chemical/crystal state, powder particle morphology, etc For the fabrication of $Mg^{11}B_2$ bulks, the major focus of this study is to control the phase purity and superconducting properties of the resultant product. We have characterized the critical current density (J_c) of $Mg^{11}B_2$ multifilament wire for the performance evaluation of isotopic boron powder.

2 | EXPERIMENTAL PROCEDURE

Three commercially available ^{11}B powders were obtained from each company and used as boron sources: American Elements (A) 99%, Cambridge (C) 99%, and Pavezyum (P) >95.5%, where the numbers refer to the nominal chemical purity, while the isotope purity was examined independently.

The phase compositions of the ^{11}B-rich powders were examined by high-resolution X-ray diffractometry (HR-XRD; ATX-G) using Cu Kα radiation. The morphology of the powder particles was characterized by scanning electron microscopy (SEM; MERLIN, Carl Zeiss). The size distribution of the ^{11}B powders was analyzed using a Mastersizer S

(Malvern Instruments, UK). The isotope ratio of ^{10}B to ^{11}B was examined using accelerator mass spectrometry (AMS) available at the Australian Nuclear Science and Technology Organization (ANSTO) on the basis of the AMS complex ANTARES (Australian National Tandem for Applied Research) equipped with the HVEE 846 Cs sputtering negative ion source and injector magnet.[26] The same isotope ratio was also determined through measurements of the neutron beam absorption in the powders using the KOWARI diffractometer in the neutron transmission (NT) mode.[27] Near edge X-ray absorption fine structure (NEXAFS) measurements at the 10D X-ray absorption spectrometer (XAS)B/L at the Pohang Accelerator Laboratory (PAL) and X-ray photoelectron spectroscopy (XPS; PHI 5000 Versa Probe (ULVAC PHI)) were introduced in order to investigate the chemical state of the ^{11}B.

For the production of bulk $Mg^{11}B_2$ superconductors, the ^{11}B-rich powder was mixed with Mg powder (100-200 mesh, 99%) in a molar ratio of Mg + 2B. After grinding properly in an agate mortar, the mixtures were pressed into cylindrical pellets (5 mm diameter and 2 mm thickness) under a pressure of 5 MPa using cold pressing equipment. The obtained pellets were sintered at 700 and 800°C under high purity argon flow (ramp rate: 5°C/min and dwell time of 1 hour). The phase composition of the thus-produced $Mg^{11}B_2$ superconductors was measured by X-ray diffraction (XRD, GBC-MMA) and dc magnetic susceptibility vs temperature was measured for determining the superconducting critical temperature of $Mg^{11}B_2$ bulk on a 9T physical properties measurement system (PPMS, Quantum Design).

Multifilamentary (12-filament) $Mg^{11}B_2$ wires have been fabricated using (P) and (C) ^{11}B powders. In this manufacturing process, the powder is dispensed into an iron tube with 6 mm OD and 4 mm ID This tube with ^{11}B has been drawn to reduce the diameter down. After drawing to the proper size, that is, 1.5 mm, these monofilaments are then stacked into 12-subelement arrays inside an iron outer tube or sheath and then drawn to the final size.

The transport J_c values were measured as a function of applied magnetic field in a 9 T magnet at 4.2 K in a liquid helium He flow cryostat using a four-probe technique, with currents up to 250 A. The temperature was measured on a current lead positioned close to the sample. The voltage taps were 14 mm apart, and the voltage criterion used was 0.1 μV cm^{-1}. In some cases, the criterion of 1 μV cm^{-1} was used for comparison.

3 | RESULTS AND DISCUSSION

The most critical property for nuclear applications, the isotope content of ^{10}B for the three ^{11}B-rich powders, is shown in Table 1. In this work, we have measured the isotope content precisely and efficiently in boron powders for the first time with high accuracy cross-checking results using two independent methods. The two methods used for determining the amount of ^{10}B impurity are in general agreement, although the NT method has larger uncertainties related to the finite accuracy of the compaction density determination. The Cambridge ^{11}B (C) powder contains the largest amount of ^{10}B, and the American Elements ^{11}B (A) powder has the lowest ^{10}B content, while the Pavezyum ^{11}B (P) powder is in the middle, with content between the C powder and the A powder. In all cases, the actual ^{11}B purity was within the nominal 99%, while American Element powder was as pure as 99.4%.

TABLE 1 Isotope ratio and size distributions of American Elements ^{11}B powder (A), Cambridge ^{11}B powder (C), and Pavezyum ^{11}B powder (P)

Materials	Isotope composition, at % of ^{10}B (AMS, NT)	Mean size	
		D [3, 2][a] (μm)	D [4, 3][b] (μm)
American Elements	0.57 ± 0.02 0.40 ± 0.10	57.2 ± 0.07	115.21 ± 0.14
Cambridge	1.04 ± 0.04 0.90 ± 0.10	21.74 ± 0.27	67.74 ± 0.84
Pavezyum	0.74 ± 0.04 0.75 ± 0.10	2.68 ± 0.03	23.47 ± 0.29

Abbreviations: AMS, accelerator mass spectrometry; NT, neutron transmission mode.

[a]D [3, 2] = The volume/surface mean (also called the Sauter mean) diameter.[31]

[b]D [4, 3] = The mean diameter over volume (also called the DeBroukere mean).[32]

Figure 1 presents the XRD patterns of the three different ^{11}B powders. All major diffraction peaks can be defined

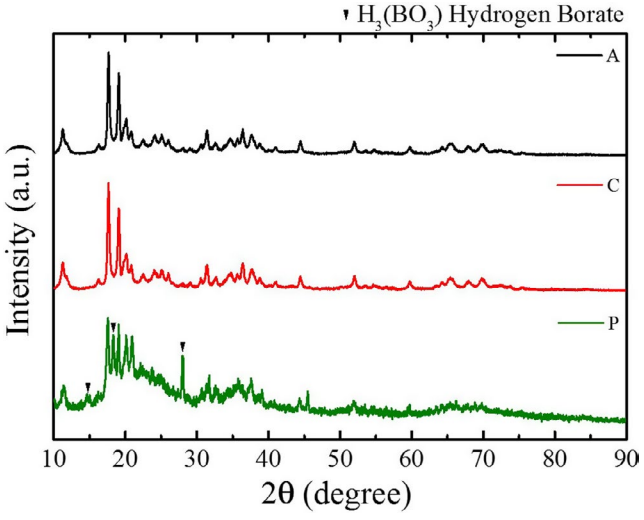

FIGURE 1 HR-XRD patterns of American Elements (A), Cambridge (C), and Pavezyum (P) ^{11}B-rich powders

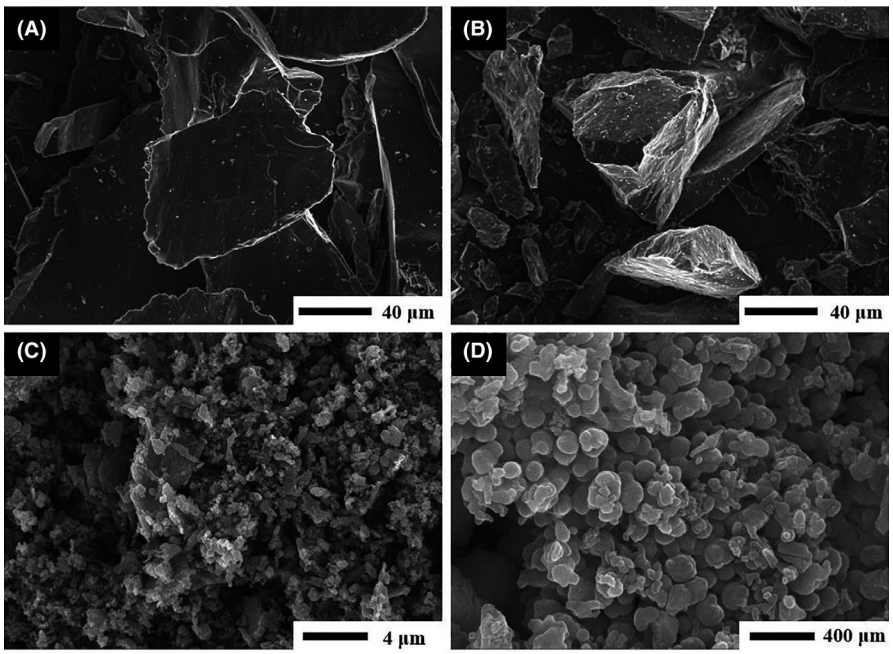

FIGURE 2 SEM images of three different ^{11}B powders: (A) American Elements ^{11}B, (B) Cambridge ^{11}B, and (C, D) Pavezyum ^{11}B-rich powders

as β-rhombohedral boron (JCPDS: 31-0207).[28] In the case of P, there is a significant peak broadening compared to A and C, and it has an impurity identified as hydrogen borate ($H_3(BO_3)$). β-rhombohedral phases have been formed in all powders but powder P has impurity defined as hydrogen borate. We assume that impurities are originated from the synthesis procedures.

Peak broadening indicates that the P powder has the lowest crystallinity and the smallest crystallite domain size among three different ^{11}B powders.[29,30] The microstructure of the ^{11}B powders is shown in Figure 2. As seen in the SEM images, the A and C powders are micrometer-sized powders with plate-shaped particles, while P powder has spherical shaped particles of sub-micrometer-size. The mean sizes for the three ^{11}B-rich powders are shown in Table 1. The *D* [3, 2] and *D* [4, 3] results (explained in Table 1) indicate that the A powder has the largest particle size, followed by the C powder, and the P powder has the smallest particle size. The particle size analysis results are consistent between the XRD results and the SEM observations.

The accurate chemical bonding and structure of the ^{11}B powders were determined by NEXAFS and XPS. The B K-edge NEXAFS spectra of the ^{11}B powders can be explained by $s + p_z$ (π* transitions) and $p_x + p_y$ (σ* transitions).[33,34] The results found for the individual powders where the peaks as shown in Figure 3 have similar tendencies. The peak at 191.8 eV in the NEXAFS spectra is derived from the typical B-B bonding of the elemental boron, and the sharp peak correlated with the bonding of metallic boron at 194.4 eV in the π* resonance region is indexed as the transition of B 1*s* electrons to the unoccupied B $2p_z$ orbital.[35,36] For the σ* resonance region, there is a significantly broad peak from 197 to 207 eV revealed in P boron. Although ^{11}B powders do not have significant structure in the σ* resonance region, it is suggested that ^{11}B powder in P has an amorphous or low crystallite structure.[37,38]

Supplementary Information on the chemical bonding of these samples can be derived from core level X-ray photoemission spectroscopy. Figure 4 presents the core level photoemission spectra for the three sorts of ^{11}B powders. Three peaks are observed in all boron 1*s* signals, as shown in Figure 4A-C, which have peak positions of 187.1-187.2, 188.4, and 191-192 eV.[31] The two low-binding-energy groups, around 187 and 188 eV, are most likely from B-B bonds in the ^{11}B powders.[39,40] The weak signal peak (191-192 eV) is

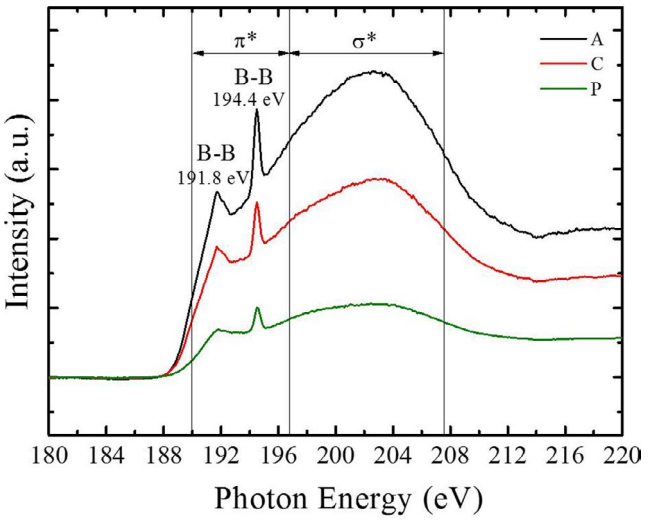

FIGURE 3 Near edge X-ray absorption fine structure spectroscopy spectra across the boron K-edge absorption spectrum. Curve A is American Elements ^{11}B, curve C is Cambridge ^{11}B, and curve P is Pavezyum^{11}B-rich powders

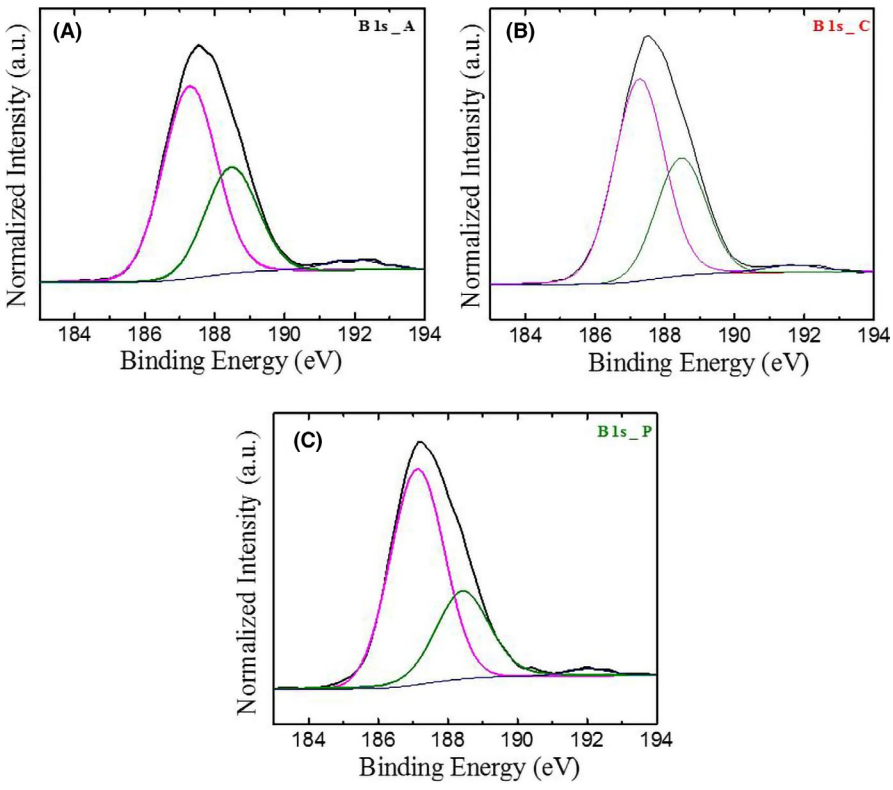

FIGURE 4 Boron 1*s* core level XPS spectra of ^{11}B powders: (A) American Elements ^{11}B, (B) Cambridge ^{11}B, and (C) Pavezyum^{11}B-rich powders

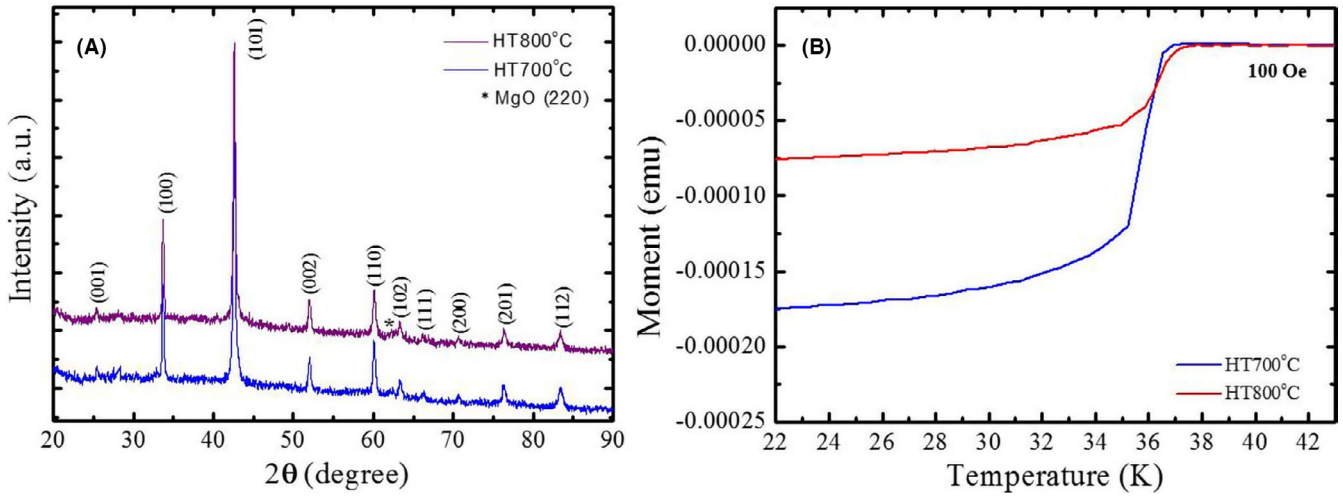

FIGURE 5 Characteristics of $Mg^{11}B_2$ bulk superconductor sintered at 700 and 800°C: (A) XRD results for HT 700°C and HT 800°C. The (hkl) labels show $Mg^{11}B_2$ reflections. (B) Temperature dependence of the zero-field-cooled demagnetizations at 100 Oe

involved with the oxidation of ^{11}B or associated with the oxidized ^{11}B in the higher energy region.[41]

It has been reported that the properties of the boron powder as a starting precursor such as crystallinity, purity, and particle size distribution, significantly influence and determine the fundamental electromagnetic and superconducting properties of the reacted MgB_2 products.[42-45] In particular, the crystalline phase is believed to require high temperature for a full reaction between Mg and B, which decreases the superconducting current paths. The same was confirmed in our characterization of the studied powders. $Mg^{11}B_2$ samples fabricated with powders C and A with strong evidence of crystallinity and plate-shaped large particle size resulted in resistive behavior even sintered at 700 and 800°C [not shown here]. Therefore, the powder P with the smallest particle size and lower crystallinity was selected in order to improve the reaction rate and reduce the sintering temperature for the complete formation of $Mg^{11}B_2$.[46] The XRD analysis in Figure 5A shows that the main phase was $Mg^{11}B_2$, while MgO was also present as a second phase impurity in both bulk samples sintered at 700 and 800°C.

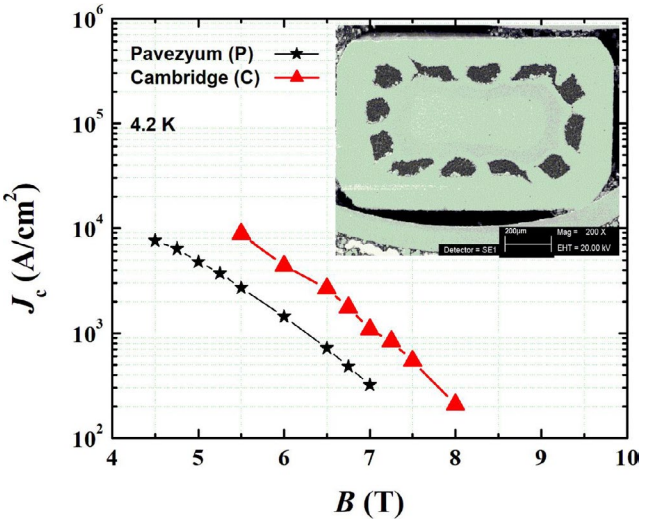

FIGURE 6 Transport J_c vs B for 12-filament MgB_2 wire samples sintered at 800°C using ^{11}B sourced from Pavezyum (P) and Cambridge (C) at 4.2 K. SEM image of the cross-sectional view of the 12-filament $Mg^{11}B_2$ wire is shown in the inset

$Mg^{11}B_2$ bulk samples fabricated from ^{11}B (P) sintered at two temperatures 700 and 800°C were used for the characterization of superconducting properties. Figure 5B shows the zero-field-cooled (ZFC) demagnetization results measured at 100 Oe for the $Mg^{11}B_2$ samples as functions of temperature, with clear normal-superconducting transitions observed in all samples with critical temperature (T_c) values of 36.5 K (HT 700°C sample) and 36.9 K (HT 800°C sample). Compared to the reported results,[47] the lower T_c in the present samples could be possibly due to the presence of a small amount of MgO and other impurity phases.

However, the critical current density (J_c) is of the most importance in the performance characteristics of our $Mg^{11}B_2$ wires. In our previous study,[48,49,50] we synthesized $Mg^{11}B_2$ using the same ^{11}B (P) powder and systematically studied the sintering process and critical current density of low activation $Mg^{11}B_2$ superconductors in bulk and wire form. It is of interest to compare the achieved J_c in our samples with the best reported results.

Kim et al[43] reported a comprehensive analysis on various sources of natural boron powders and compared the electronic and superconducting performance of mono- and multi-filament wires samples. MgB_2 wire doped with malic acid made from amorphous, high purity and nano size natural boron showed the J_c as high as 2.5×10^4 A cm^{-2} at 4.2 K and 10 T (tesla), even for a sintering temperature as low as 600°C. This performance is the best J_c reported so far in in situ processed wires. The undoped low activation $Mg^{11}B_2$ wires were recently manufactured by using the isotopic ^{11}B (P) powder.[49] The J_c value of this isotopic wire showed 2×10^4 A cm^{-2} at 4.2 K and 5 T which is relatively lower than the J_c value (10^5 A cm^{-2} at 4.2 K and 5 T) for the natural boron based high activation undoped MgB_2 wire reported in the ref. 43.

In the comparison with the best examples of the high activation MgB_2 superconductors, our low activation isotopic $Mg^{11}B_2$-wires lack their performance in terms of J_c; however, several ways of the performance improvements are envisaged (especially low- and high-field J_c). From the viewpoint of optimizing processing costs and critical properties, it is evident that the boron precursor powder properties such as purity, phase and size are extremely important for the performance of the wire. In case of ^{11}B powder the current production route (the Mosisson process using isotopic boric acid) determines the morphology of the ^{11}B powder that appears to be inferior against the natural boron powder produced by gaseous diborane processing reported previously.[51] With certain modification of the ^{11}B powder processing, for example, incorporating additional processing steps in order to achieve better purity, less crystallinity and smaller particle size, some significant performance improvements are expected. More improvements can be achieved through the use of the doping approach.

Figure 6 shows the transport J_c as a function of magnetic field of 12-filament MgB_2 wires using the 11B powder sourced from Pavezyum (P) and Cambridge (C) at 4.2 K. The inset displays the cross-sectional orientation of the multi-filamentary wire just to show the structure and morphology of the wire filament. It has to be noted that the transport J_c measurements cannot be done at low field (<4.5 T) due to the limitation of current flow (250 A) into the probe, therefore high field results can be seen in Figure 6. $Mg^{11}B_2$ wire using (P) show higher J_c at 4.2 K compared to that for wire using (C). The steeper slope of J_c vs B is observed for (P) wires compared to that for (C) wires. The value of B(10^4) [where the field at which J_c reaches to 10^4 A/cm^2] was enhanced from 4.5 to 5.5 T in P wire compared to C wire which may be originated from smaller grain size of low crystalline ^{11}B (P) powder and better grain connectivity in multifilamentary MgB_2 wire.

Thus, based on the results of the $Mg^{11}B_2$-based performance using different sources, at least one powder, ^{11}B (P), has enormous potential which demonstrated that the superconducting wires produced from it can provide typical superconducting properties that can satisfy the requirements for critical temperature and current carrying capability with further possibilities for improvement.

4 | CONCLUSIONS

Our analysis has demonstrated that all three of the ^{11}B powders that we studied have the β-rhombohedral crystalline phase but slightly different ^{10}B isotope content as an impurity. The boron powder from Pavezyum has proved to have the most optimal combination of properties amongst the three suppliers of the precursor powder for production of $Mg^{11}B_2$

bulk and 12-filament $Mg^{11}B_2$ wires: smallest particle size, the lowest crystallinity among the three ^{11}B powders, and an acceptable ^{11}B isotope purity of 99.25%. The wire using (P) shows three times higher J_c at particular magnetic field, that is, 5.5 T. This combination of properties resulted with in the formation of $Mg^{11}B_2$ superconductor media of better performance, both magnetic and transport critical current density and critical temperature.

When considered in connection with practical manufacturing of superconducting wires and cables for possible use in future fusion reactors, with the current improvement of the performance, the $Mg^{11}B_2$-based superconducting wires proved their potential to be used in the next generation liquid-helium-free superconducting fusion magnets (specifically in the low magnetic field coils, that is, PF and CC) to replace the more expensive, higher neutron activation, and lower operation temperature NbTi-based superconductors. In the view of steady progress in the area, the current study provides the first real demonstration and sets a reference point for $Mg^{11}B_2$-based superconducting wires.

ACKNOWLEDGEMENTS

This work is supported by the Australian Research Council (ARC) Linkage project (LP160101784) and Australian Centre for Neutron Scattering (ACNS) through its user access program (Proposal no. ZIAI073441). Higher degree research scholarship for H.J. is supported by the Australian Nuclear Science and Technology Organization (ANSTO), Australia. A. K. thanks the Researchers Supporting Project (RSP-2019/127), King Saud University, Riyadh, Saudi Arabia, for the support. M. M. thanks an internal funding project of the University of Osijek (ZUP-2018), Croatia. This work was partly performed at the Queensland node of the Australian National Fabrication Facility (ANFF), a company established under the National Collaborative Research Infrastructure Strategy to provide nano- and micro-fabrication facilities for Australian researchers.

ORCID

Hyunseock Jie https://orcid.org/0000-0002-6637-7789
Anvar Valiyaparambil Abdulsalam https://orcid.org/0000-0003-1264-6442
Keun Hwa Chae https://orcid.org/0000-0003-3894-670X
Hyung-il Choi https://orcid.org/0000-0001-9452-7257
Arend Nijhuis https://orcid.org/0000-0002-1600-9451
Aslam Khan https://orcid.org/0000-0002-7906-5653
Md. Shahriar A. Hossain https://orcid.org/0000-0002-7291-9281

REFERENCES

1. Devred A, Backbier I, Bessette D, Bevillard G, Gardner M, Jong C, et al. Challenges and status of ITER conductor production. Supercond Sci Technol. 2014;27:044001.
2. Boutboul T, Readman P, Viladiu E, Losasso M, Caballero J, Abou-Yehia J, et al. Status of the procurement of the European superconductors for the ITER magnets. IEEE Trans Appl Supercond. 2014;24:6001004.
3. Mitchell N, Devred A. The ITER magnet system: configuration and construction status. Fus Eng Des. 2017;123:17–25.
4. Hishinuma Y, Kikuchi A, Shimada Y, Kashiwai T, Hata S, Yamada S, et al. Development of MgB_2 superconducting wire for the low activation superconducting magnet system operated around core D-T plasma. Fus Eng Des. 2015;98-99:1076–80.
5. Sato S, Iida H, Nishitani T. Evaluation of shutdown gamma ray dose rates around the duct penetration by three-dimensional Monte Carlo decay gamma ray transport calculation with variance reduction method. J Nucl Sci Technol. 2002;39:1237–46.
6. Noda T, Takeuchi T, Fujita M. Induced activity of several candidate superconductor materials in a tokamak-type fusion reactor. J Nucl Mater. 2004;329–333:1590–3.
7. Hishinuma Y, Yamada S, Sagara A, Kikuchi A, Takeuchi T. Development of low activation superconducting material for the feedback coil operated around core D-T plasma. IAEA Fus Eng Conf. 2010;43:FT/P1-8.
8. Seidel P. Applied superconductivity: Handbook on devices and applications. London: John Wiley & Sons, 2015; v. 2.
9. Tsiskarishvili GP, Lundström T, Tegenfelt TJ, Dolidze V, Tsagareishvili GV. Isotope effect in β−rhombohedral boron. AIP Conf Proc. 1991;280:231.
10. Chkhartishvili L. Isotopic effects of boron (Review). Trends Inorg Chem. 2009;11:105–67.
11. Sears VF. Neutron scattering lengths and cross sections. Neutron News. 1992;3(3):29.
12. Nikolić RJ, Conway AM, Reinhardt CE, Graff RT, Wang TF, Deo N. 6:1 aspect ratio silicon pillar based thermal neutron detector filled with ^{10}B. Appl Phys Lett. 2008;93:133502.
13. Eisterer M, Zehetmayer M, Tönies S, Weber HW, Kambara M, Babuet HN, et al. Neutron irradiation of MgB_2 bulk superconductors. Supercond Sci Technol. 2002;15:L9–12.
14. Wilke RHT, Bud'ko SL, Canfield PC. Systematic study of the superconducting and normal-state properties of neutron-irradiated MgB_2. Phys Rev B. 2006;73:134512.
15. Putti M, Braccini V, Ferdeghini C, Gatti F, Manfrinetti P, Marreet D, et al. Neutron irradiation of $Mg^{11}B_2$: from the enhancement to the suppression of superconducting properties. Appl Phys Lett. 2005;86:112503.
16. Mooring FP, Monahan JE, Huddleston CM. Neutron cross sections of the boron isotopes for energies between 10 and 500 keV. Nucl Phys. 1966;82:16–32.
17. Hinks DG, Jorgensen JD. The isotope effect and phonons in MgB_2. Physica C. 2003;385:98–104.
18. Tarantini C, Aebersold HU, Braccini V, Celentano G, Ferdeghini C, Ferrando V, et al. Effects of neutron irradiation on polycrystalline $Mg^{11}B_2$. Phys Rev B. 2006;73:134518.
19. Dou SX, Soltanian S, Horvat J, Wang XL, Zhou SH, Ionescu M, et al. Enhancement of the critical current density and flux pinning of MgB_2 superconductor by nanoparticle SiC doping. Appl Phys Lett. 2002;81:3419–21.
20. Kim JH, Yeoh WK, Qin MJ, Xu X, Dou SX. Enhancement of in-field JcJc in MgB2/FeMgB2/Fe wire using single- and multiwalled carbon nanotubes. Appl Phys Lett. 2002;89:122510-1–122510-3.
21. Yeoh WK, Kim JH, Horvat J, Xu X, Qin MJ, Dou SX, et al. Control of nano carbon substitution for enhancing the critical current density in MgB_2. Supercond Sci Technol. 2006;19:596–9.

22. Ribeiro A, Budko SL, Petrovic C, Canfield PC. Carbon doping of superconducting magnesium diboride. Physica C. 2003;384:227–36.
23. Mickelson W, Cummings J, Han WQ, Zettl A. Effects of carbon doping on superconductivity in magnesium diboride. Phys Rev B. 2002;65:052505-1–052505-3.
24. Yamamoto A, Shimoyama J, Ueda S, Iwayama I, Horii S, Kishio K. Effects of B4C doping on critical current properties of MgB2 superconductor. Supercond Sci Technol. 2005;18:1323–8.
25. Kim JH, Zhou S, Hossain MSA, Pan AV, Dou SX. Carbohydrate doping to enhance electromagnetic properties of MgB_2 superconductors. Appl Phys Lett. 2006;89:142505.
26. Tuniz C, Fink D, Hotchkis M, Jacobsen G, Lawson E, Smith A, et al. The antares AMS centre: a status report. Radiocarbon. 1995;37(2):663–73.
27. Kirstein O, Luzin V, Garbe U. The strain-scanning diffractometer Kowari. Neutron News. 2009;20:34–6.
28. Liu G, Yin L, Niu P, Jiao W, Cheng H. Visible-light-responsive β-rhombohedral boron photocatalysts. Angew Chem Int Ed. 2013;52:6242–5.
29. Ungár T. Microstructural parameters from X-ray diffraction peak broadening. Script Mater. 2004;51:777–81.
30. Cullity BD, Stock SR. Elements of X-ray diffraction. 3rd ed. New York: Prentice Hall PTR; 2001.
31. Wang D, Fan LS. Fluidized bed technologies for near-zero emission combustion and gasification. Oxford: Woodhead Publishing Series in Energy; 2013, p. 42–76.
32. Horiba Scientific, A guidebook to particle size analysis 2016 [cited 2019 May 30]. http://www.horiba.com/us/en/scientific/products/particle-characterization
33. Li D, Bancroft GM, Fleet ME. B K-edge XANES of crystalline and amorphous inorganic materials. J Electron Spectrosc. 1996;79:71–3.
34. Peter R, Bozanic A, Petravic M, Chen Y, Fan LJ, Yang YW. Formation of defects in boron nitride by low energy ion bombardment. J Appl Phys. 2009;106:083523.
35. Petravic M, Peter R, Kavre I, Li LH, Chen Y, Fan L-J, et al. Decoration of nitrogen vacancies by oxygen atoms in boron nitride nanotubes. Phys Chem Chem Phys. 2010;12:15349–53.
36. Jankowski AF, Jimenez I, Hayes JP, Shuh DK, Tong WM, Sutherland D, et al. Near-edge X-ray absorption fine structure examination of chemical bonding in sputter deposited boron and boron-nitride films. Mat Res Soc Symp Proc. 1996;437:207–10.
37. Zhang D, Davalle DM, O'Brien WL, McIlroy DN. The chemical composition of as-grown and surface treated amorphous boron carbon thin films by means of NEXAFS and XPS. Surf Sci. 2000;461:16–22.
38. Fleet ME, Liu X. Boron K-edge XANES of boron oxides: tetrahedral B-O distances and near-surface alteration. Phys Chem Min. 2001;28:421–7.
39. Li L, Li LH, Chen Y, Dai XJ, Xing T, Petravic M, et al. Mechanically activated catalyst mixing for high-yield boron nitride nanotube growth. Nano Res Lett. 2012;7:417.
40. Moudler JF, Stickle WF, Sobol PE, Bomben KD. Handbook of X-ray photoelectron spectroscopy. Waltham: Perkin-Elmer; 1992.
41. Feng B, Zhang J, Zhong Q, Li W, Li S, Li H, et al. Experimental realization of two-dimensional boron sheets. Nat Chem. 2016;8:563–8.
42. Xu X, Yeoh WK, Zhang Y, Dou SX. Improved J_c of MgB_2 superconductor by ball milling using different media. Supercond Sci Technol. 2006;19:L47–50.
43. Kim JH, Heo Y, Matsumoto A, Kumakura H, Rindfleisch M, Tomsic M, et al. Comparative study of mono- and multi-filament MgB_2 wires with different boron powders and malic acid addition. Supercond Sci Technol. 2010;23:075014.
44. Xu X, Qin MJ, Konstantinov K, Santos DI, Yeoh WK, Kim JH, et al. Effect of boron powder purity on superconducting properties of MgB_2. Supercond Sci Technol. 2006;19:466–9.
45. Chen SK, Yates KA, Blamire MG, MacManus-Driscoll JL. Strong influence of boron precursor powder on the critical current density of MgB_2. Supercond Sci Technol. 2005;18:1473–7.
46. Cai QI, Guo Q, Liu Y, Ma Z, Li H, Qiu W, et al. Doping-induced isotopic $Mg^{11}B_2$ bulk superconductor for fusion application. Energies. 2017;10:409.
47. Margadonna S, Muranaka T, Prassides K, Maurin I, Brigatti K, Ibberson RM, et al. Phase inhomogeneities and lattice expansion near T_c in the $Mg^{11}B_2$ superconductor. J Phys Condens Matter. 2001;13:L795–802.
48. Cheng F, Liu YC, Ma ZQ, Hossain MSA, Somer M. Sintering process and critical current density of low activation (MgB_2)-B-11 superconductors from low temperature to high temperature. Physica C. 2016;527:9–13.
49. Qiu W, Jie H, Patel D, Lu Y, Luzin V, Devred A, et al. Improvement in the transport critical current density and microstructure of isotopic $Mg^{11}B_2$ monofilament wires by optimizing the sintering temperature. Sci Rep. 2016;6:636660.
50. Cheng F, Liu YC, Ma ZQ, Hossain MSA, Somer M. Improved Superconducting properties in the $Mg^{11}B_2$ low activation superconductor prepared by low-temperature sintering. Sci Rep. 2016;6:25498.
51. Barua S, Hossain MSA, Ma ZQ, Patel D, Mustapić M, Somer M, et al. Superior critical current density obtained in MgB_2 bulks through low-cost carbon-encapsulated boron powder. Script Mater. 2015;104:37–40.

How to cite this article: Jie H, Luzin V, Zaman M, et al. Evaluation of isotopic boron (^{11}B) for the fabrication of low activation $Mg^{11}B_2$ superconductor for next generation fusion magnets. *J Am Ceram Soc*. 2020;00:1–8. https://doi.org/10.1111/jace.17156